Atmos. Chem. Phys., 24, 5549–5565, 2024
https://doi.org/10.5194/acp-24-5549-2024

Atmospheric Chemistry and Physics
Open Access
EGU

Secondary organic aerosols derived from intermediate-volatility n-alkanes adopt low-viscous phase state

Tommaso Galeazzo[1], Bernard Aumont[2], Marie Camredon[2], Richard Valorso[2], Yong B. Lim[3], Paul J. Ziemann[4,5], and Manabu Shiraiwa[1]

[1]Department of Chemistry, University of California, Irvine, Irvine, California 92625, USA
[2]Univ Paris Est Creteil and Université Paris Cité, LISA, CNRS, 94010 Créteil, France
[3]Mobile Source Laboratory Division, California Air Resources Board, Riverside, California 92507, USA
[4]Department of Chemistry, University of Colorado Boulder, Boulder, Colorado 80309, USA
[5]Cooperative Institute for Research in Environmental Sciences (CIRES), University of Colorado Boulder, Boulder, Colorado 80309, USA

Correspondence: Manabu Shiraiwa (m.shiraiwa@uci.edu)

Received: 8 January 2024 – Discussion started: 18 January 2024
Revised: 26 March 2024 – Accepted: 27 March 2024 – Published: 14 May 2024

Abstract. Secondary organic aerosol (SOA) derived from n-alkanes, as emitted from vehicles and volatile chemical products, is a major component of anthropogenic particulate matter, yet the chemical composition and phase state are poorly understood and thus poorly constrained in aerosol models. Here we provide a comprehensive analysis of n-alkane SOA by explicit gas-phase chemistry modeling, machine learning, and laboratory experiments to show that n-alkane SOA adopts low-viscous semi-solid or liquid states. Our study underlines the complex interplay of molecular composition and SOA viscosity: n-alkane SOA with a higher carbon number mostly consists of less functionalized first-generation products with lower viscosity, while the SOA with a lower carbon number contains more functionalized multigenerational products with higher viscosity. This study opens up a new avenue for analysis of SOA processes, and the results indicate few kinetic limitations of mass accommodation in SOA formation, supporting the application of equilibrium partitioning for simulating n-alkane SOA formation in large-scale atmospheric models.

1 Introduction

Secondary organic aerosol (SOA) is ubiquitous in the atmosphere, affecting climate, air quality, and public health (Pöschl and Shiraiwa, 2015; Jimenez et al., 2009). It is generally formed by multigenerational oxidation of volatile organic compounds (VOCs) emitted by both anthropogenic and biogenic sources followed by condensation of semi-volatile oxidation products into the particle phase (Ziemann and Atkinson, 2012; Kroll and Seinfeld, 2008). As an important class of SOA precursors, there is a growing attention given to intermediate-volatility organic compounds (IVOCs), which can partition to the gas phase upon dilution of primary organic aerosols after fresh emission sources such as vehicle tailpipes, combustion of fossil and fuel oils, and volatile chemical products (Robinson et al., 2007; McDonald et al., 2018). The inclusion of IVOCs in the model simulations helps to reduce the gap between model simulations and field observations of SOA (de Gouw et al., 2011; Li et al., 2022; Zhao et al., 2016).

SOA can adopt different particle phase states (liquid, amorphous semi-solid, and glassy solid), depending on their chemical composition, relative humidity, and temperature (Virtanen et al., 2010; Petters et al., 2019; Reid et al., 2018; Renbaum-Wolff et al., 2013) and also evolving with regards to chemical aging and photochemistry (Baboomian et al., 2022). SOA phase state plays an important role in a number of atmospheric multiphase processes (Shiraiwa et al., 2017).

The occurrence of glassy SOA in the free troposphere can impact activation pathways of ice crystals and cloud droplets (Knopf and Alpert, 2023). Slow diffusion in viscous particles induces kinetic limitations in heterogeneous and multiphase reactions (Zhang et al., 2018; Zhou et al., 2019; Shiraiwa et al., 2011), affecting long-range transport (Shrivastava et al., 2017; Mu et al., 2018). The timescale of SOA partitioning can be prolonged in viscous particles (Schervish and Shiraiwa, 2023), retarding uptake of semi-volatile compounds and mixing of different particle populations (Ye et al., 2016). The particle phase state also modulates SOA growth to cloud condensation nuclei sizes, affecting the cloud life cycle (Zaveri et al., 2022). While the phase states of SOA generated by biogenic VOCs such as terpenes and isoprene have been extensively studied (Virtanen et al., 2010; Petters et al., 2019; Renbaum-Wolff et al., 2013; Baboomian et al., 2022; Zhang et al., 2018), those derived from IVOCs are hardly investigated and remain poorly constrained.

Viscosity (η) is a dynamic property that characterizes the particle phase state, which can be derived from the glass transition temperature (T_g) of the constituting species (Koop et al., 2011). Several structure–activity relationships models have been developed to predict the T_g of an organic compound using various molecular properties including molar mass, the atomic O : C ratio (Shiraiwa et al., 2017), elemental composition (DeRieux et al., 2018), and volatility (Li et al., 2020; Zhang et al., 2019). A method was developed to predict SOA viscosity from the T_g-scaled Arrhenius plot of fragility by considering the Gordon–Taylor mixing rule and hygroscopic growth of SOA particles (DeRieux et al., 2018; Shiraiwa et al., 2017). The T_g compositional parametrization (CP) and the viscosity prediction method have been applied to high-resolution mass spectrometry data of various types of SOA including toluene SOA (DeRieux et al., 2018), SOA generated by diesel fuels (Song et al., 2019), β-caryophyllene SOA (Maclean et al., 2021), and SOA generated by surrogate VOC mixtures by healthy and stressed plants (Smith et al., 2021), agreeing well with viscosity measurements. However, CP substantially overestimated viscosity measurements of indoor surface films which are mostly composed of unsaturated high-molar-mass compounds such as triglycerides (O'Brien et al., 2021). CP considers neither molecular structure nor functionality explicitly, representing a limitation of this method. Galeazzo and Shiraiwa (2022) overcame this limitation by developing a machine-learning-based model, tgBoost, with an application of cheminformatics "molecular embeddings" that retains detailed information on atomic composition, molecular structure, and connectivity. The main novel feature introduced by tgBoost is the model capability to predict different T_g values for structural isomers and a high sensitivity of T_g to various functional groups, consistent with viscosity measurements for functionalized compounds (Rothfuss and Petters, 2017; Grayson et al., 2017).

Long-chain linear alkanes (n-alkanes) are representative IVOCs and account for a substantial fraction of non-methane hydrocarbons in urban air as mainly emitted from anthropogenic activities such as vehicle exhausts and incomplete fuel combustion (Li et al., 2022). Gas-phase oxidation of n-alkanes by OH radicals can trigger the formation of SOA with high yields, as observed in laboratory experiments (Aimanant and Ziemann, 2013a; Lim and Ziemann, 2009b; Srivastava et al., 2022) and field observations (Gentner et al., 2012; Li et al., 2022). Gas-phase oxidation pathways of n-alkanes are relatively well understood and successfully simulated by detailed gas-phase chemistry modeling (Aumont et al., 2012; La et al., 2016), but the chemical composition of n-alkane SOA has only been characterized well for the C_{16} n-alkane (Ranney et al., 2023) and the phase state and viscosity of alkane SOA are unknown. Therefore, the n-alkane SOA system provides an ideal benchmark for the investigation of the interplay of chemical composition, particle phase state, and kinetic limitations influencing SOA growth and evolution.

In this study, we implemented tgBoost in an explicit gas-phase chemistry model, GECKO-A (Generator for Explicit Chemistry and Kinetics of Organics in the Atmosphere), to investigate the complex interplay of chemical composition, kinetic partitioning, and the phase state of n-alkane SOA generated under dry and high-NO_x conditions. The GECKO-A model is one of the most comprehensive generators of gas-phase chemical schemes to date, as it automatically generates detailed gas-phase chemical mechanisms involving thousands to millions of oxidation products from a given VOC precursor based on established reaction pathways and structure–activity relationships (Aumont et al., 2012; La et al., 2016). The simulations were conducted with a variable effective mass accommodation coefficient to consider potential kinetic limitations in amorphous semi-solid particles (Shiraiwa and Pöschl, 2021). The simulated results were compared with chamber experimental data on SOA yields (Lim and Ziemann, 2009b) as well as new measurements on thermal desorption temperatures and functional-group distributions.

2 Methods

2.1 Model simulations

We applied the Generator for Explicit Chemistry and Kinetics of Organics in the Atmosphere (GECKO-A) (Aumont et al., 2012; La et al., 2016) to obtain detailed reaction schemes of gas-phase OH oxidation of n-alkanes along with rate constants. The GECKO-A generator used for the oxidation of linear n-alkanes treats the chemistry of peroxy (RO_2) and alkoxy (RO) radicals. Under high-NO_x conditions, RO_2 radicals mainly react with NO and NO_2, in order to form closed-shell compounds or RO radicals, which undergo reaction with O_2, unimolecular decomposition (i.e., C–

C bond breaking), or isomerization, generating stable compounds and/or new RO_2 radicals. The detailed protocol for such mechanism generation is available in previous studies (Aumont et al., 2013, 2005, 2012; La et al., 2016). In this study, the generated chemical schemes include the description of the formation of organic species up to four generations. Species with vapor pressure below 10^{-13} atm are assumed to be of low enough volatility to completely partition to the condensed phase, and their gas-phase chemistry is then not generated in the mechanism to reduce the mechanism (La et al., 2016). The number of species treated in the model was $\sim 10^4$ species for dodecane (C_8H_{18}), which increases to $\sim 10^5$ species for heptadecane ($C_{17}H_{36}$).

The latest structure–activity relationships are treated for the chemistry of organic compounds with an OH radical (Jenkin et al., 2018b, a, 2019) and the bimolecular reactions of peroxy radicals (Jenkin et al., 2019), as well as alkoxy radical decomposition and H migration reaction rates (Vereecken and Peeters, 2009; La et al., 2016). The vapor pressures of semi-volatile species were estimated by using Nannoolal's group contribution method (Nannoolal et al., 2008) implemented in GECKO-A, as described in detail in Valorso et al. (2011). The model treats unimolecular particle-phase reactions including the cyclization of hydroxyketones and dehydration of cyclic hemiacetals to form dihydrofurans (La et al., 2016). The model does not treat autoxidation and dimerization in the gas phase, but these processes should be minor pathways during n-alkane oxidation in the presence of high NO_x as the reaction of peroxy radicals with NO_x should be dominant (Praske et al., 2018; Pye et al., 2019); thus, their absence from GECKO-A chemical schemes should not have major impacts on the simulated results.

These explicit chemical mechanisms were implemented in a box model to simulate the multigenerational oxidation of n-alkanes, partitioning of oxidation products into the particle phase based on their vapor pressures, and vapor wall loss to mimic chamber experiments (La et al., 2016). We replicated the experimental conditions used in Lim and Ziemann (2009b) to generate SOA from OH oxidation of C_8–C_{17} n-alkanes under high-NO_x conditions in the presence of non-volatile dioctyl sebacate (DOS) seed particles with a particle radius of 150 nm and mass loading of 200 $\mu g\,m^{-3}$. Temperature was held constant at 295.15 K, pressure was set at 1 atm, and RH was fixed at 0.5 %. Photolysis frequencies were calculated based on the cross sections and quantum yields as described in Aumont et al. (2005) and the photonic flux of blacklight lamps. Each simulation ran for 1 h, and the time evolution of species concentration was computed through a two-step method that solves stiff ordinary differential equations (Verwer, 1994; Verwer et al., 1996). To investigate effects of mass concentrations, we also simulated experiments of n-alkane photooxidation under high-NO_x conditions with low mass loadings by Presto et al. (2010). The number concentration of seed particles with a particle diameter of 200 nm was $\sim 5000\,cm^{-3}$, corresponding to the mass concentration of $\sim 20\,\mu g\,m^{-3}$. Initial mixing ratios of n-alkane and NO_x were in the range of 3–99 ppb and 1–5 ppm, respectively, as reported in Presto et al. (2010), and these conditions were applied in the model.

The box model accounts for mass transfer kinetics of organic species between gas and particle phases. Partitioning follows Raoult's law at equilibrium and partitioning kinetics as described by the gas–particle mass transfer coefficient with the Fuchs–Sutugin approach (Seinfeld and Pandis, 2016). For the base case scenario, we fixed the mass accommodation coefficient (α) to be 1 based on molecular dynamics simulations (Julin et al., 2014), assuming particles are low-viscous liquids without kinetic limitations of bulk diffusion. To account for potential kinetic limitations in viscous particles, we applied an effective mass accommodation coefficient (α_{eff}) that is a function of volatility and bulk diffusivity (Shiraiwa and Pöschl, 2021):

$$\alpha_{eff} = \alpha_s \frac{1}{1 + \frac{\alpha_s \omega C^0}{4 D_b \rho_p} \cdot \frac{r_p}{5} \cdot 10^{-12} \frac{g\,cm^{-3}}{\mu g\,m^{-3}}}, \quad (1)$$

where α_s is the surface accommodation coefficient assumed to be 1, ω ($cm\,s^{-1}$) is the mean thermal velocity of the organic compound in the gas phase, r_P (cm) is the particle radius, ρ_p ($g\,cm^{-3}$) is the particle density, and C^0 ($\mu g\,m^{-3}$) is the pure compound saturation mass concentration. D_b ($cm^2\,s^{-1}$) is bulk diffusivity as simulated by the conversion of viscosity as detailed below. α_{eff} values are shown as a function of D_b and vapor pressure p^o in Fig. A3a. We accounted for a reversible gas-to-chamber wall partitioning of gases and assumed a fixed first-order deposition rate constant of $5 \times 10^{-4}\,s^{-1}$ based on experimental observations and previous modeling studies (Krechmer et al., 2016; La et al., 2016; Lim and Ziemann, 2009b). A desorption rate constant from the wall to the gas phase was derived by using a parameter of $C_w/M_w\gamma_w$ of 9 $\mu mol\,m^{-3}$ for n-alkanes and 120 $\mu mol\,m^{-3}$ for oxidation products based on chamber observations (Matsunaga and Ziemann, 2010), as discussed in La et al. (2016). Potential concentration gradients in the particle phase are not resolved explicitly, and SOA particles are assumed to be homogeneously well-mixed.

The glass transition temperatures (T_g) of organic compounds were predicted by the machine-learning-based model tgBoost (Galeazzo and Shiraiwa, 2022) and the parametrization based on elemental composition (DeRieux et al., 2018; Li et al., 2020). The implementation of the compositional parametrization in the GECKO-A box model was done in Galeazzo et al. (2021) with a thorough description of all the equations, assumptions, and steps adopted for the implementation of this viscosity estimation method. In this study, we implemented tgBoost, a newly developed machine learning model for better predictions of T_g. tgBoost is a powerful model that can discern compositional isomers by functionality and predict the glass transition temperature of an organic compound i ($T_{g,i}$) with an uncertainty of

±18.3 K using the canonical SMILES (simplified molecular input line entry system) notation of a molecule (Galeazzo and Shiraiwa, 2022). We have implemented a pipeline (i.e., gecko2vec) into GECKO-A to predict T_g of compounds from the chemical mechanism in a fast and computationally efficient manner. The gecko2vec pipeline executes three main steps: first, it translates the IDs of the compounds of interest of the GECKO-A mechanism into the respective canonical SMILES notations (translation step); second, it transforms the canonical SMILES notations into the respective molecular embeddings (i.e., unique 300-dimensional numerical representations of molecules; embedding step); and, finally, the pretrained tgBoost model and its weights are loaded and used to predict the T_g of each species (prediction step). Within the box model, the T_g of total SOA particles ($T_{g,org}$) resulting from the combination of its organic component and water mixture is computed using the Gordon–Taylor equation (Dette et al., 2014; Koop et al., 2011; Zobrist et al., 2008). $T_{g,org}$ can be converted to viscosity based on the Vogel–Fulcher–Tammann approach assuming a fragility parameter of 10 (DeRieux et al., 2018). Viscosity is further converted into bulk diffusivity using the fractional Stokes–Einstein equation with a fractional parameter of 0.93 and an effective molecular radius of 0.5 nm (Evoy et al., 2019). For both model simulations with CP and tgBoost, the particle number concentration is assumed to remain constant (coagulation is not treated), while the particle radius evolves following the partitioning of organic compounds.

2.2 Laboratory experiments

SOA particles were generated from OH oxidation of C_8–C_{17} n-alkanes in a 5.9 m^3 Teflon environmental chamber filled with clean air under high-NO_x conditions in the presence of non-volatile DOS seed particles, as described in detail elsewhere (Lim and Ziemann, 2009b). Briefly, 1 ppm of n-alkane, 10 ppm of methyl nitrite, and 10 ppm of NO were added to the chamber from a glass bulb, and $\sim$ 200–400 µg m^{-3} of seed particles were added from an evaporation–condensation apparatus. Relatively high-mass concentrations of seed particles were used so that semivolatile compounds would condense to particles, minimizing vapor deposition to chamber walls (Zhang et al., 2014; Matsunaga and Ziemann, 2010). Blacklights covering two of the chamber walls were then turned on for 60 min to form OH radicals by methyl nitrite photolysis (Atkinson et al., 1981). The amount of n-alkane reacted was measured by collecting Tenax® samples before and after the experiment and analyzing by gas chromatography with flame ionization detection (GC-FID). Aerosol volume concentrations were measured using a scanning mobility particle sizer (SMPS; Docherty et al., 2005) and converted to an SOA mass formed using a density of 1.06 g cm^{-3}. SOA mass yields (mass of SOA formed / mass of n-alkane reacted) were calculated from the measured SMPS mass (corrected for particle wall loss using the $\sim$ 20 % h^{-1} decay in mass after the lights were turned off) and the GC-FID analyses. The final SOA mass concentrations were in the range of $\sim$ 300–6000 µg m^{-3} depending on precursors (Lim and Ziemann, 2009b). The SOA yields measured in these experiments were reported previously (Lim and Ziemann, 2009b), but regarding a recent comparison of the accuracy of our SMPS measurements with filter sampling, the values reported here are higher by a factor of 1.24 (Bakker-Arkema and Ziemann, 2021).

A temperature-programmed thermal desorption (TPTD) method was also used to measure thermal desorption temperatures of DOS that was present as seed particles in n-alkane SOA. Particles were sampled directly from the chamber into a thermal desorption particle beam mass spectrometer (Tobias et al., 2000), where they were formed into a beam inside an aerodynamic lens, were transported into a high vacuum chamber, and impacted on a copper rod vaporizer that was coated with a non-stick polymer and cooled to −40 °C. Note that compounds with a vapor pressure of $< 10^{-5}$ torr are estimated to undergo negligible evaporation with the residence time of $\sim$ 0.2 s in the aerodynamic lens (Tobias et al., 2000). After sampling for 30 min, the vaporizer was warmed by room air to −5 °C and then heated at 2 °C min^{-1} to 200 °C. Compounds desorbed according to volatility and entered a quadrupole mass spectrometer, where they were ionized by 70 eV electrons prior to mass analysis. In one recent n-hexadecane experiment, the composition of nitrate, hydroxyl, carbonyl (ketone + aldehyde), carboxylic acid, ester, and peroxide functional groups in SOA was measured using derivatization–spectrophotometric methods, with the number of -CH_2- groups calculated by difference (Ranney et al., 2023). We note that in that experiment the SOA yield measured by filter sampling was nearly identical to the one we measured previously after applying the above correction.

3 Results and discussion

3.1 SOA yields and viscosity

Figure 1 shows comparisons of measurements and modeling for (a) SOA yields, (b) functional-group distributions, (c) N : C ratios, and (d) O : C ratios. Figure 1a shows the measured yields of SOA generated from the oxidation of n-alkanes (C_nH_{2n+2}; carbon number n = 8–17) (Lim and Ziemann, 2009b). The model base case (black line) with a mass accommodation coefficient of 1 for all species represents no kinetic limitations in the particle phase, and the results are similar to previous simulations performed by La et al. (2016). Vapor wall loss was considered based on experimental observations and previous modeling studies (Krechmer et al., 2016; La et al., 2016; Lim and Ziemann, 2009b), which is important to account for as no wall loss would lead to a significant overestimation of SOA yields, as shown by the dotted black line and discussed in detail in La et al. (2016). Both experimental and simulated SOA yields increase with an in-

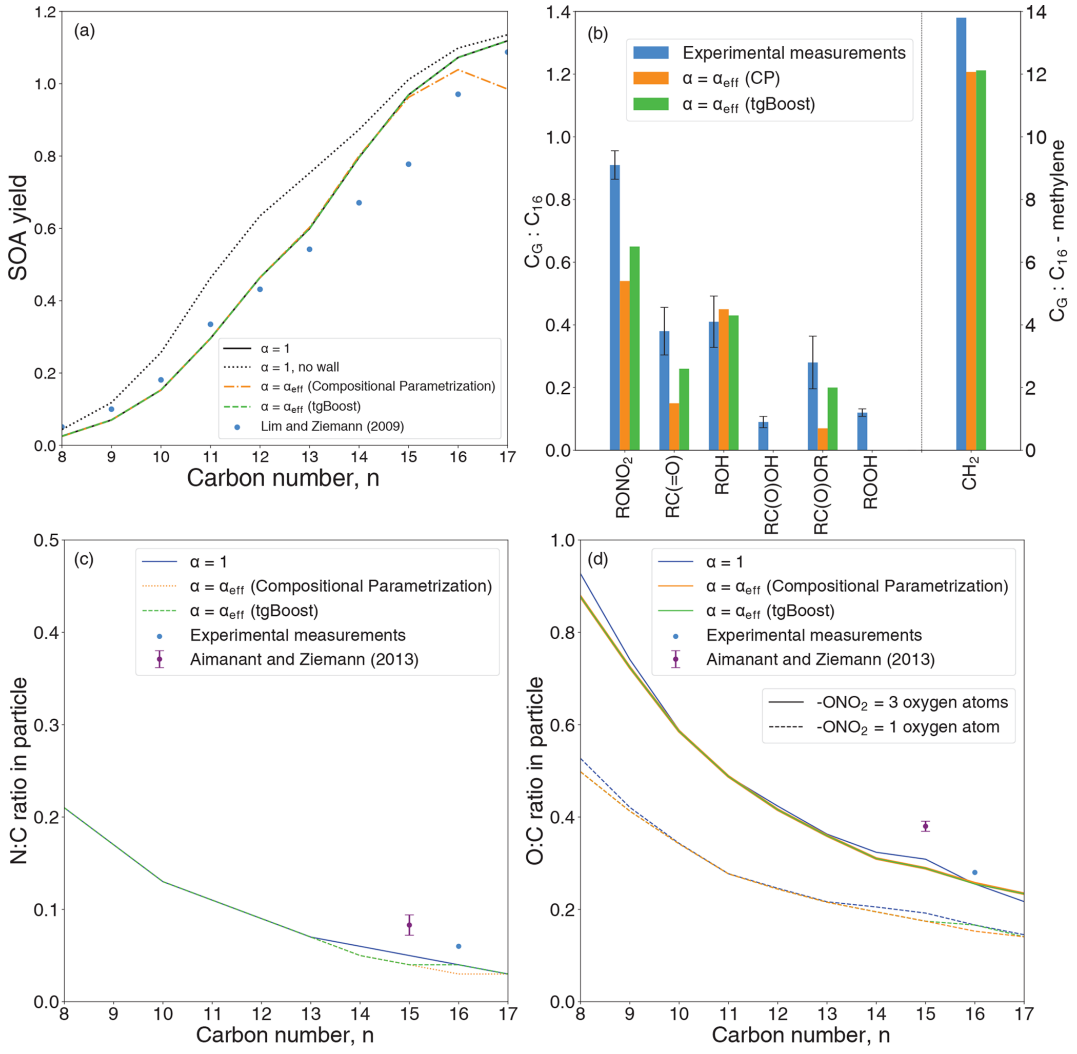

Figure 1. **(a)** Yields of SOA generated from OH oxidation of linear n-alkanes as measured by Lim and Ziemann (2009b) (markers) and modeled by the GECKO-A box model (lines). The black line represents the base case with a mass accommodation coefficient (α) of 1. The dashed lines represent simulations with an effective mass accommodation coefficient (α_{eff}) as a function of bulk diffusivity from tgBoost (green) and the compositional parametrization (orange). **(b)** Simulated functional-group distributions of n-hexadecane ($C_{16}H_{34}$) oxidation products in the particle phase. The blue bars represent experimental measurements. The green and orange bars represent GECKO-A box model simulations with α_{eff} with tgBoost and the compositional parametrization, respectively. **(c)** N : C and **(d)** O : C ratios in SOA formed by n-alkane oxidation simulated by the GECKO-A box model. The black line represents the base case with an α value of 1. The dashed lines represent simulations with α_{eff} with tgBoost (green) and the compositional parametrization (orange). The markers represent experimental measurements for C_{15} (Aimanant and Ziemann, 2013a) and C_{16} (Table A1).

crease in n, reflecting the decrease in volatility of the precursor and its oxidation products (Shiraiwa et al., 2014). The observed SOA yield trend is consistent with measurements by a thermal desorption particle beam mass spectrometer, showing that n-alkane SOA is composed of less oxidized products with lower volatility for precursors with a higher n (Lim and Ziemann, 2009b, a).

The overall good agreement suggests that multigenerational chemistry in the gas phase and partitioning of semi- and low-volatile products, as explicitly treated by GECKO-A box modeling, are the dominant pathway of n-alkane SOA formation under these conditions. It also suggests that peroxy radicals (RO_2) mainly react with NO_x, minimizing autoxidation and gas-phase dimerization by $RO_2 + RO_2$ reactions. Good model agreement also suggests that particle-phase oligomerization chemistry is not a dominant process, while particle-phase unimolecular reactions including cyclization of hydroxyketones and dehydration of cyclic hemiacetals forming dihydrofurans are treated in the model as they are important for the further oxidation due to the presence of a double bound in the dihydrofurans (Lim and Ziemann, 2009a; La et al., 2016). Thus, the GECKO-A model

seemingly treats all essential processes for simulations of n-alkane SOA formation under high-NO_x conditions. Note that a very recent study suggested that cyclic hemiacetals form acetal dimers in the particle phase for SOA formed from the reaction of n-hexadecane SOA and OH/NO_x (Ranney et al., 2023). In addition, particle-phase chemistry was shown to be substantial in n-alkane SOA formation under low-NO_x conditions through peroxyhemiacetal and oligomer formation (Shiraiwa et al., 2013; Ziemann and Atkinson, 2012). The impact of such particle-phase chemistry may warrant further investigations including model development and experimental studies.

To explore the potential impacts of the particle phase state on SOA formation and partitioning, we implemented an effective mass accommodation coefficient (α_{eff}) which can effectively consider kinetic limitations of bulk diffusion and also account for the effect of vapor pressure on partitioning kinetics for species with various volatilities (Shiraiwa and Pöschl, 2021). Bulk diffusivity evolves upon SOA formation, which can be derived by viscosity and T_{g} as predicted by the machine-learning-based tgBoost model (dashed green line in Fig. 1a) and the compositional parametrization (CP; dashed orange line in Fig. 1a). The simulated SOA yields with tgBoost are very similar to the base case scenario with $\alpha = 1$, while the application of the CP leads to smaller SOA yields for $n = 15$–17. These results indicate that α_{eff} is close to 1 with few kinetic limitations of bulk diffusion for most cases, although some limitations are predicted by CP for large precursors. Deviations of tgBoost and CP stem from the difference in phase state and viscosity predicted by the two methods.

Figure 2a shows the simulated viscosity and corresponding bulk diffusivity of n-alkane SOA. Notably, the two models predict contrasting trends. The simulated glass transition temperature ($T_{\mathrm{g,org}}$) of SOA is presented in Fig. A1. The CP predicts a decrease in $T_{\mathrm{g,org}}$ for C_{8-12} with the lowest $T_{\mathrm{g,org}}$ of ~ 250 K, which is likely due to a decrease of the O : C ratio (Fig. 1d) as a lower O : C ratio can lead to a decrease in T_{g} (DeRieux et al., 2018; Shiraiwa et al., 2017), followed by an increase in $T_{\mathrm{g,org}}$, with n reaching ~ 270 K with C_{17}. These values correspond to viscosity of 10^4–10^6 Pa s, indicating that n-alkane SOA adopts a viscous semi-solid phase state. The increase in viscosity for larger precursors is apparently reasonable, as their oxidation products would have a higher molar mass which would generally correspond to a higher $T_{\mathrm{g,org}}$ (Koop et al., 2011; Shiraiwa et al., 2017). Based on the Stokes–Einstein relation, bulk diffusivity would be in the range of 3×10^{-15}–10^{-12} cm^2 s^{-1}. The characteristic timescale of bulk diffusion in an average particle diameter of 300 nm can be as low as ~ 2 h (Shiraiwa et al., 2011), which is longer than the experimental timescale of 1 h. These low diffusivities and the long diffusion timescale can induce concentration gradients in the particle bulk, reducing α_{eff} and causing significant kinetic limitations that retard SOA growth, which is not consistent with the measured SOA yields.

tgBoost predicts the opposite trend, predicting a monotonic decrease in $T_{\mathrm{g,org}}$ and viscosity with an increase in n, suggesting that SOA phase state shifts from an amorphous semi-solid state ($10^2 < \eta < 10^5$ Pa s) towards a liquid-like phase state ($\eta < 10^2$ Pa s). These results are counter-intuitive as T_{g} values of n-alkanes increase with an increase in n, which can be reproduced with great precision by tgBoost (Galeazzo and Shiraiwa, 2022). The determinants explaining this unexpected trend are the chemical composition and molecular structure of the oxidation products as discussed below. The characteristic timescale of bulk diffusion is less than 1 s in a low-viscous state, and high bulk diffusivity (Shiraiwa et al., 2011) and SOA particles are expected be homogeneously well-mixed. Hence, α_{eff} remains very close to 1 with little kinetic limitation of bulk diffusion.

Unfortunately, no direct viscosity measurements of n-alkane SOA generated under high-NO_x conditions are available to date, while there are two studies of n-alkane SOA generated under NO_x-free conditions. Saukko et al. (2012) observed that n-heptadecane ($C_{17}H_{36}$) SOA with a low O : C ratio did not bounce from an impactor plate. This indicates that these particles adopted a liquid-like state, as indicated by the violet shading in Fig. 2a, which is consistent with the tgBoost prediction. Shiraiwa et al. (2013) estimated the bulk diffusivity of n-dodecane ($C_{12}H_{26}$) SOA generated without NO_x to be 10^{-12} cm^2 s^{-1} using a kinetic multilayer model to simulate the evolution of particle size distribution. While these two data points cannot be directly compared with the viscosity predictions of high-NO_x n-alkane SOA, they serve as reference data points for now, and direct viscosity or bulk diffusivity measurements of high-NO_x n-alkane SOA are warranted in future studies.

Figure 2b shows the thermal desorption profiles of DOS that was present as seed particles within the SOA formed from oxidation of the n-alkanes. Since DOS desorption involved diffusion through the SOA prior to escape into a vacuum, these profiles provided a means for probing the SOA viscosity. The peaks in the DOS profiles for the C_{8-13} and C_{14-17} n-alkanes are closely grouped, with the vaporizer temperature at ~ 80 and ~ 65 °C, respectively, with the peak for pure DOS occurring in between at ~ 72 °C. The observed decrease in desorption temperatures from low to high carbon numbers suggests an increase in the effective volatility of DOS in SOA generated from larger n-alkanes. In addition, Lim and Ziemann (2009b) have observed that C_{10} n-alkane SOA generated under high-NO_x conditions evaporates at higher temperatures compared to C_{12} and C_{15} n-alkane SOA based on total ion thermal desorption measurements. Volatility and T_{g} were shown to exhibit a clear anticorrelation (Li et al., 2020); hence, these results strongly indicate that C_{8-13} SOA has a higher T_{g} and viscosity compared to C_{13-17} SOA. Note that the C_{13} profile is bimodal with peaks at ~ 80 and ~ 65 °C (Fig. 2b), which is in line

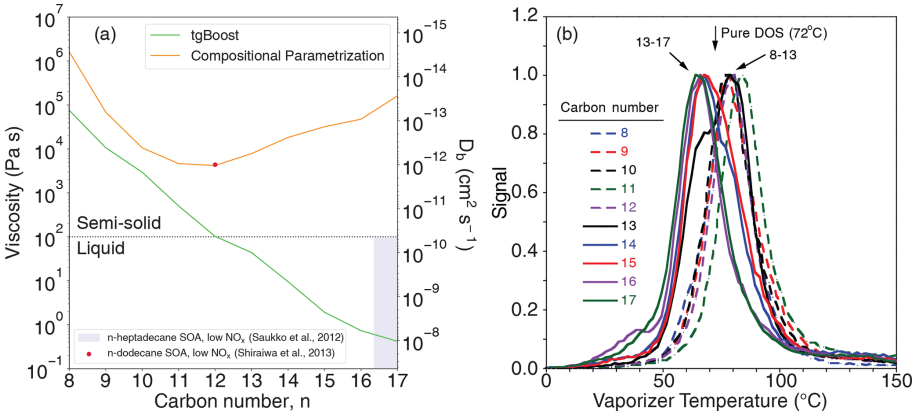

Figure 2. Phase state of n-alkane SOA. **(a)** Predicted viscosity of SOA generated from n-alkanes as computed by the GECKO-A box model with the T_g compositional parametrization (orange line) and tgBoost (green line) at the last step of the simulations ($t = 3600$ s). **(b)** Thermal desorption temperatures of dioctyl sebacate (DOS) that was present as seed particles in n-alkane SOA.

with the tgBoost prediction that the viscosity of C_{13} alkane SOA is at the edge of amorphous semi-solid and liquid phase states (Fig. 2a). These results indicate that n-alkane SOA generated by larger precursors adopt low-viscous liquid-like states, while n-alkane SOA generated by smaller precursors adopt viscous semi-solid states, in agreement with tgBoost predictions. The major strength of tgBoost is that it considers molecular structure and functionality for T_g predictions, while the compositional parametrization does not account for this effect, leading to intuitive but erroneous predictions.

3.2 Chemical composition of SOA

Figure 1 also shows the simulated (c) N : C and (d) O : C ratios of SOA with $\alpha = 1$ (black line) and $\alpha = \alpha_{eff}$ with T_g determined with tgBoost (green line) or the compositional parametrization (orange line). The N : C ratio is very similar among all simulations, being ~ 0.2 for C_8 and decreasing progressively to ~ 0.03 with each addition of a carbon atom in the precursor. O : C ratios were calculated in two different ways by treating a (nitrate-ONO_2) group to contain either three (solid lines) or one (dashed lines) oxygen atom. One oxygen atom is also considered because O : C ratios reported from aerosol mass spectrometer measurements generally treat a nitrate group the same as a hydroxyl group, since they have the same effect on the oxidation state (Farmer et al., 2010). Similar to the N : C ratio, there is a constant decrease in the O : C ratio of SOA with an increasing n, which is consistent with previous measurements for n-pentadecane ($C_{15}H_{32}$) SOA (Aimanant and Ziemann, 2013a) and n-hexadecane ($C_{16}H_{34}$) SOA in this study, even though the simulated values are $\sim 45\,\%$ and $15\,\%$ lower than the measured N : C and O : C ratios, respectively. The discrepancies are likely due to errors in modeling gas–wall partitioning and gas–particle partitioning. The difference may also be caused by missing processes in the model such as the reactive uptake of oxidants and particle-phase chemistry.

We measured functional-group distributions in n-hexadecane SOA using derivatization-spectrophotometric methods described in Aimanant and Ziemann (2013b), as shown in Fig. 1b and summarized in Table A1. Experimental measurements report a high presence of -CH_2- (13.81) and -ONO_2 (0.91), followed by ROH (0.41), RC(=O) (0.38), and RC(=O)OR (0.28), with the average measured number of groups per C_{16} molecule in parenthesis. Figure 1b includes simulation results by GECKO-A with CP and tgBoost, showing overall satisfactory agreement. The simulated results with tgBoost show excellent agreement for hydroxyl and methylene groups, while the simulated nitrates and carbonyls (ketones + aldehydes) are lower than the measurements. The simulation by CP also has a similar trend but with a significantly lower presence of nitrates, carbonyls, and esters.

Figure 3a shows the top 15 oxidation products in the particle phase formed by the oxidation of n-hexadecane simulated by the GECKO-A box model with tgBoost. Note that positional isomers are lumped into one species and that the five species in the first row constitute a majority ($\sim 86\,\%$) of SOA mass. The simulated SOA is composed mostly by first-generation products including alkyl nitrates, hydroxynitrates, and hydroxyketones. There is also a significant presence of second- and third-generation products such as esters and dinitrates. We also predicted multi-functionalized decomposition products including smaller chain hydroxy nitrates and alkyl lactones as well as particle-phase products from the cyclization of hydroxyketones and dehydration of cyclic hemiacetals to form dihydrofurans. A very recent study by Ranney et al. (2023) measured n-hexadecane oxidation products under high-NO_x conditions, finding that alkyl nitrates, hydroxyl nitrates, hydroxyl carbonyls, cyclic hemiacetals, and cyclic hemiacetal nitrates were major products. These com-

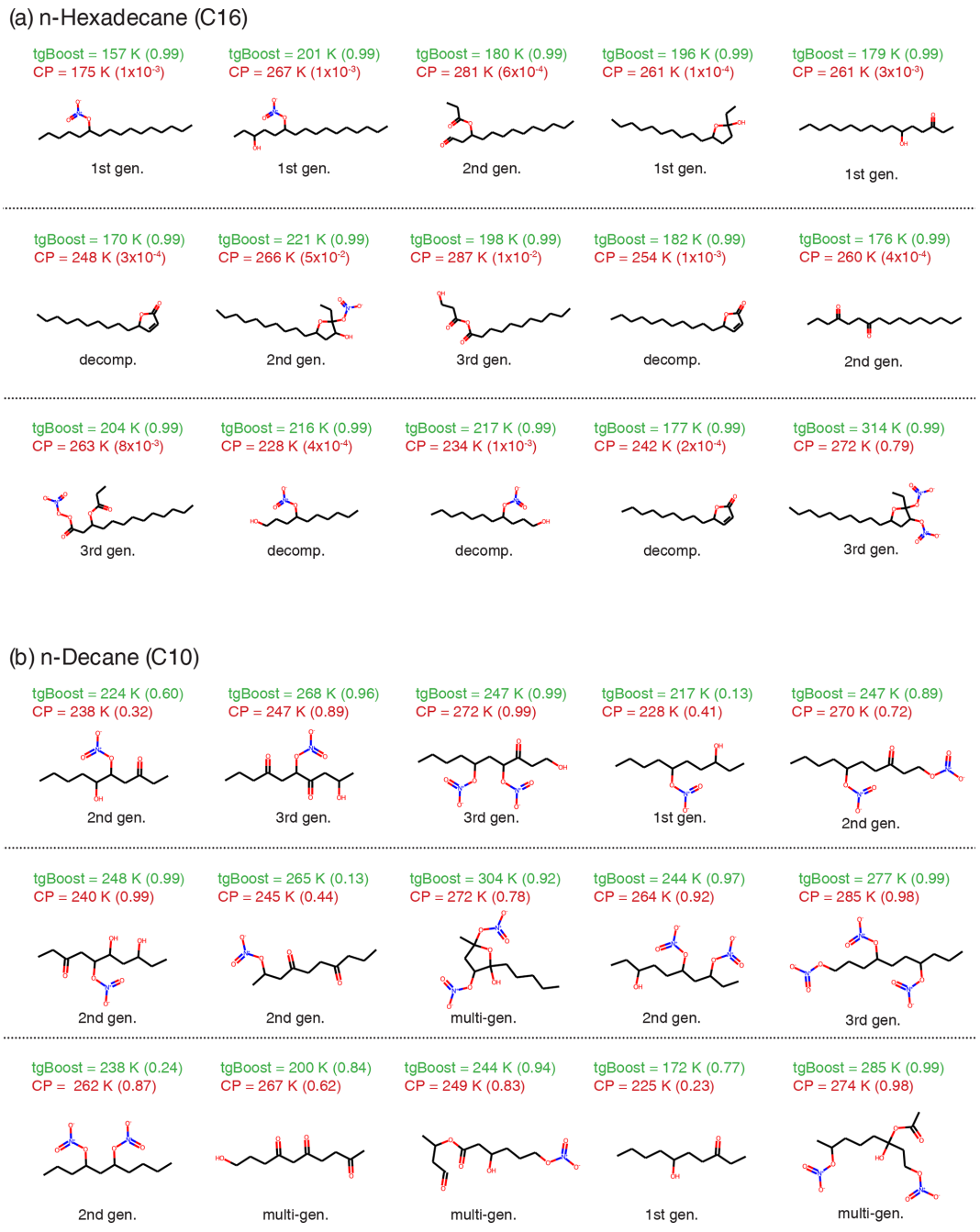

Figure 3. Molecular composition of oxidation products of n-alkanes under high-NO_x conditions in the particle phase. Top 15 SOA contributors with the highest concentrations in **(a)** n-hexadecane ($C_{16}H_{34}$) SOA and **(b)** n-decane ($C_{10}H_{32}$) simulated by GECKO-A with an effective mass accommodation coefficient (α_{eff}) with tgBoost. The species are reported in descending concentrations from left to right and from top to bottom. Positional isomers are lumped into one species. Listed values are T_g as calculated by tgBoost and CP and α_{eff} values at the end of the simulation (3600 s) in parentheses. Types of compounds are also noted (first-, second-, and third-generation products, decomposition products).

pounds are also major products as shown in Fig. 3a, suggesting that GECKO-A simulated n-alkane oxidation very well. There are notable differences in molecular composition for SOA simulated by CP compared to tgBoost (Fig. A2): the major compounds are first-generation single- and multi-functionalized products, followed by some second- and third-generation products, without decomposition products in the top species.

The T_g simulated by both methods for each compound is listed in Fig. 3. Overall tgBoost predicts T_g values be-

tween 157–221 K, which are much lower compared to CP, especially with significant differences for organic nitrates and multi-functionalized species. As tgBoost considers the molecular structure, functional group, and atomic interconnectivity of a molecule, it should make better predictions for multi-functionalized compounds based on the presence of different functional groups. CP is based on elemental composition, and it predicts a high T_g for compounds with high molar mass, predicting the same T_g for isomers. In addition, the CP for CHON compounds was developed based on T_g values mainly estimated from their melting points, as there are a limited number of CHON compounds with measured T_g available. The T_g of organic nitrates is especially scarce, and future T_g measurements for organic nitrates are desired to improve T_g parametrizations. For these reasons, CP overestimates T_g for oxidation products of n-alkane with a long chain on average by ~ 66 K compared to tgBoost, overpredicting SOA viscosity as shown in Fig. 2a.

Figure 3 also lists α_{eff} values, showing that they are very close to 1 for tgBoost, with SOA being a low-viscous liquid with little kinetic limitations in mass accommodation. Additional oxidation products with lower concentrations are listed in Fig. A3, and their α_{eff} values remain also close to 1. In contrast, as CP predicts the SOA phase state to be a viscous amorphous semi-solid, α_{eff} values for semi-volatile compounds become significantly smaller, kinetically limiting mass accommodation. This decrease in α_{eff} is larger for compounds with higher volatility, so compounds have a higher re-evaporation rate on viscous particles with a lower rate of bulk diffusion (Shiraiwa and Pöschl, 2021) (Fig. A3). α_{eff} values for lower-volatility compounds remain high, as they exhibit much lower desorption rates and are less likely to re-evaporate, even if their diffusion into the bulk is slow. Consequently, SOA simulated with CP mainly consists of later-generation products with higher functionalization and molar masses.

Figure 3b shows the top 15 oxidation products of n-decane ($C_{10}H_{26}$) as predicted by GECKO-A with tgBoost. SOA is mostly composed of second- and third-generation products with multiple functional groups including nitrates, ketones, and alcohols. These highly oxidized products have T_g in the range of 225–304 K, with similar predictions by CP and tgBoost. This is consistent with previous studies that demonstrated successful applications of CP in predicting the measured viscosity of SOA derived from biogenic and other relatively small precursors (DeRieux et al., 2018; Smith et al., 2021; Baboomian et al., 2022). These results are consistent with total ion thermal desorption profiles of n-alkane SOA formed in the presence of NO_x (Lim and Ziemann, 2009b): C_{10} SOA was observed to have a broad single peak around ~ 75 °C, indicating the presence of low-volatility multigenerational products; in contrast, C_{12} and C_{15} SOA exhibited two peaks with one larger peak at a lower temperature, corresponding to first-generation products, and another smaller peak for multigenerational products. The phase state of n-decane SOA is predicted to be semi-solid, but kinetic limitations are not strong as α_{eff} values for most compounds are only slightly reduced from 1.

3.3 Effects of mass loadings on viscosity

The use of mass loadings in chamber experiments higher than ambient conditions assured that the condensation of semi-volatile vapors to suspended particles is a dominant process over vapor wall deposition (Zhang et al., 2014; Matsunaga and Ziemann, 2010). Chamber experiments of n-alkane photooxidation under high-NO_x conditions were also conducted with lower mass loading by Presto et al. (2010), who measured temporal evolution of SOA yields as shown in Fig. 4a. SOA yields are increased with an increase in SOA mass concentrations, which is consistent with SOA absorptive partitioning theory (Pankow, 1994). The oxidation of larger precursors leads to higher SOA yields, in agreement with Lim and Ziemann (2009b) as presented in Fig. 1a. As shown with solid lines, the GECKO-A box model simulated experimental observations of SOA yields very well.

Figure 4b depicts the simulated SOA viscosity. We observed the same trend as Fig. 2a with the lowering of viscosity upon an increase in carbon number n. The SOA phase state is predicted to be semi-solid for a low n, while it is expected to be liquid for a high n. The predicted viscosity is about 1 order of magnitude higher compared to Fig. 2a. Lower mass loadings suppress partitioning of higher-volatility compounds, resulting in higher viscosity, as condensation would be dominated by lower-volatility compounds with a higher T_g (Jain et al., 2018; Champion et al., 2019; Grayson et al., 2016; DeRieux et al., 2018).

3.4 Atmospheric implications

The phase state and viscosity of SOA formed by IVOCs have been largely unknown and unexplored. We demonstrated in this study that SOA derived from small and middle-sized n-alkanes (C_{12} and smaller) mostly consists of multigenerational oxidation products adopting an amorphous semi-solid state, while larger n-alkane SOA are mainly composed of first-generation lightly oxidized products with one or two functional groups adopting a low-viscous liquid state. This result is counter-intuitive, as it has been established that a higher molar mass would lead to higher glass transition temperature and, hence, higher viscosity (Koop et al., 2011; Shiraiwa et al., 2017). In fact, the viscosity of biogenic SOA follows this trend: the viscosity of isoprene (C_5H_8) SOA is reported to be lower than monoterpene ($C_{10}H_{16}$, such as α-pinene and limonene) SOA (Renbaum-Wolff et al., 2013; Zhang et al., 2019), while oxidation products of sesquiterpene ($C_{15}H_{24}$) increase the viscosity of SOA (Smith et al., 2021), which is captured by empirical parametrizations based on elemental composition (DeRieux et al., 2018; Li et al., 2020). In contrast, n-alkane SOA exhibits an opposite

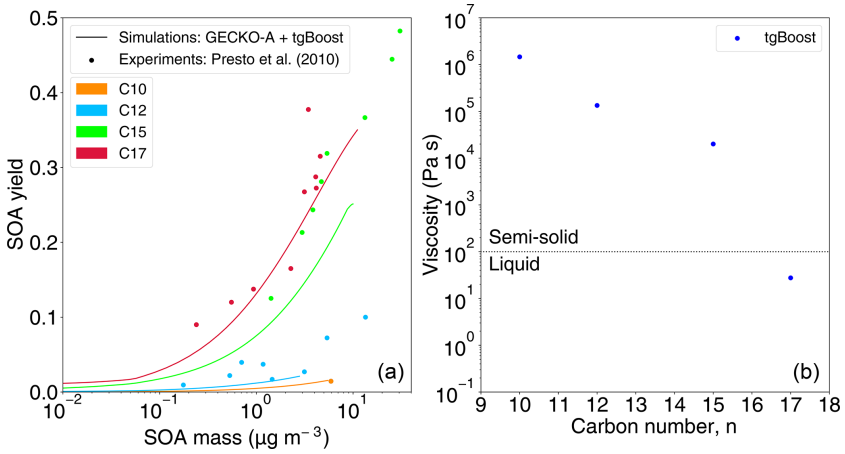

Figure 4. Effects of mass loadings on SOA yields and viscosity. **(a)** SOA yields from photooxidation of n-decane (C10), n-dodecane (C12), n-pentadecane (C15), and n-heptadecane (C17) under high-NO_x conditions as a function of SOA mass concentration, as measured in Presto et al. (2010) (markers) and as modeled by the GECKO-A box model combined with tgBoost (lines). **(b)** SOA viscosity as modeled by the GECKO-A box model combined with tgBoost.

trend, as indicated by thermal desorption measurements that show that DOS in SOA formed by the oxidation of large n-alkanes has higher volatility. Hence, the SOA has lower viscosity, due to the enhanced presence of less functionalized first-generation products (Li et al., 2020; Zhang et al., 2019). This trend is successfully predicted by GECKO-A combined with the machine-learning-based model tgBoost, which emphasizes the importance of the consideration of functionality and molecular structure in accurate predictions of T_g. The relationship between viscosity and composition is also reflected in the atomic O : C and N : C ratios of n-alkane SOA, which decrease monotonically upon an increase in the carbon number of the n-alkane, since a higher oxidation state and functionalization can increase T_g (DeRieux et al., 2018; Koop et al., 2011; Shiraiwa et al., 2017; Saukko et al., 2012).

IVOCs have gained growing attention for their better characterization of urban air quality, as they represent an important source of SOA as shown by chamber experiments (Aimanant and Ziemann, 2013a; Lim and Ziemann, 2009b) and as observed in field observations (Gentner et al., 2012; Li et al., 2022; Robinson et al., 2007; McDonald et al., 2018). While a few large-scale aerosol models treat IVOC SOA in order to achieve better agreement with ambient measurements (de Gouw et al., 2011; Li et al., 2022; Zhao et al., 2016), IVOC SOA is still highly uncertain in terms of chemical composition and particle phase state and model parameters and treatments for SOA formation and partitioning are poorly constrained. Our study provides critical insights into these aspects, showing that n-alkane SOA formation under high-NO_x conditions (as is usually the case for ambient urban air) is dominated by gas-phase chemistry followed by partitioning. As the generated SOA particles adopt a low-viscous state, there are few kinetic limitations of mass accommodation and bulk diffusion, which supports the application of equilibrium SOA partitioning in the boundary layer. While the experiments and modeling were conducted for dry conditions in this study, the phase state and viscosity of ambient n-alkane SOA would be expected to be even lower under humid conditions due to hygroscopic growth and water acting as a plasticizer. Note that further experiments and model simulations are required for different conditions for the middle and upper free troposphere, as viscosity is expected to become higher under low temperatures.

It is notable that the combination of tgBoost and the GECKO-A box model successfully simulates SOA yields, functional-group distributions, and the phase state. This new model represents a unique and comprehensive tool for simulating the formation, partitioning, and chemical evolution of SOA, opening up a new avenue for analyzing the complex interplay of gas-phase chemistry and particle-phase processes and composition in SOA for the detailed analysis and interpretation of laboratory experiments and field observations. In addition, we propose to pursue the application of this model as a basis for the development of a detailed master mechanism of multiphase aerosol chemistry as well as for the derivation of simplified but realistic parametrizations for air quality and climate models. In regional and global air quality models, it is challenging and computationally very expensive to treat complex SOA multiphase processes. Thus, such processes should be treated in an efficient but effective way, and the new model shall serve as a benchmark for the development of simplified SOA descriptions.

Appendix A

Table A1. Experimental and simulated functional-group (FG) distributions and O : C and N : C ratios of SOA generated from C_{16} oxidation by OH in the presence of high NO_x.

FG/C_{16} molecule	Experimental	Simulated (tgBoost)	Simulated (CP)
Nitrate	0.91	0.65	0.54
Carbonyl	0.38	0.26	0.15
Hydroxyl	0.41	0.43	0.45
Carboxyl	0.09	0.0	0.0
Ester	0.28	0.2	0.07
Peroxide	0.12	0.01	0.0
Methylene	13.81	12.12	12.07
O : C	0.28	0.25	0.25
N : C	0.06	0.04	0.03
H : C	1.85	–	–
MW	294	–	–
Density ($g\,cm^{-3}$)	1.10	1.06	1.06

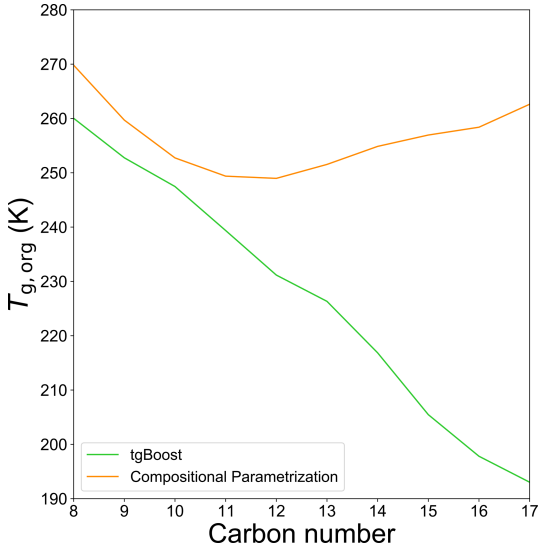

Figure A1. Predicted $T_{g,org}$ of SOA generated from n-alkanes as computed by the GECKO-A box model with the T_g compositional parametrization (orange line) and tgBoost (green line) at the last step of the simulations ($t = 3600$ s).

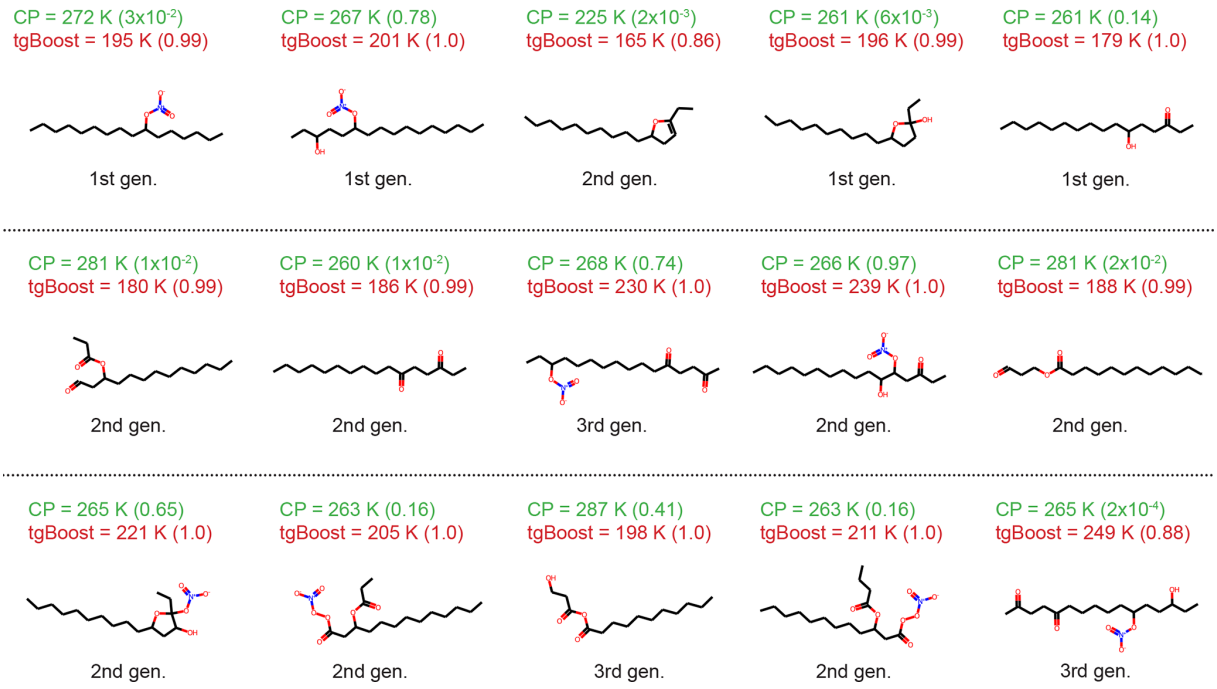

Figure A2. Top 15 species with the highest concentrations in oxidation products of n-hexadecane ($C_{16}H_{34}$) under high-NO_x conditions simulated by GECKO-A with an effective mass accommodation coefficient (α_{eff}) with the compositional parametrization. The species are reported in descending concentrations from left to right and from top to bottom. Listed values are T_g as calculated by tgBoost and CP and α_{eff} values at the end of the simulation (3600 s) in parentheses. Types of compounds are also noted (first-, second-, and third-generation products, decomposition products).

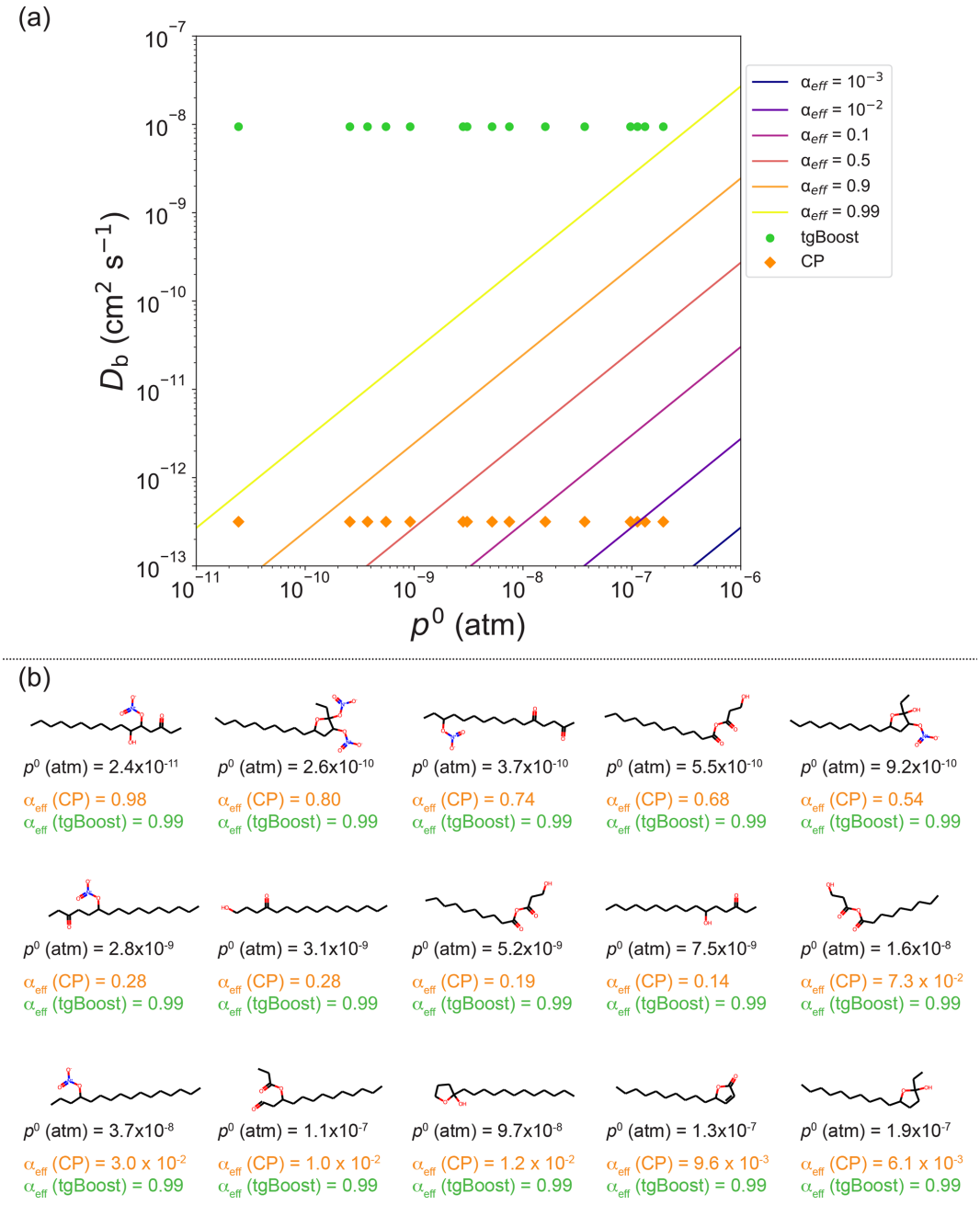

Figure A3. **(a)** α_{eff} isolines as a function of bulk diffusivity D_{b} and saturation vapor pressure p^{o} of semi-volatile species. **(b)** Selection of various representative SOA contributors produced during the oxidation of n-hexadecane. The species are ordered by decreasing vapor pressure. The reported α_{eff} values for each SOA contributor are calculated for D_{b} estimated with tgBoost ($D_{\mathrm{b}} = 1 \times 10^{-8}$ cm^2 s^{-1}) and CP ($D_{\mathrm{b}} = 3 \times 10^{-13}$ cm^2 s^{-1}). The values of α_{eff} for the selected species are reported as points in the top panel. It shows that for the liquid-like state estimated with the tgBoost configuration, α_{eff} tend towards 1 for all species. This behavior is not observed in the amorphous semi-solid state estimated using the CP model configuration for species with a p^{o} value above 10^{-9} atm. For the simulated conditions, species with a p^{o} value between 10^{-8} and 10^{-6} atm are of low enough volatility to partition between the particle and gas phases at equilibrium. For species in that volatility range, no mass transfer limitation is observed with the tgBoost configuration, unlike the CP configuration. Using the CP configuration, the most volatile SOA contributors are subjected to a substantial mass transfer limitation and are therefore mainly eliminated by gas-phase oxidation or wall deposition.

Code and data availability. The simulation data may be obtained from the corresponding author upon request. The tgBoost model is available on GitHub (https://github.com/U0M0Z/tgpipe, Galeazzo, 2024) and online (https://azothai.ps.uci.edu/, Galeazzo and Shiraiwa, 2022).

Author contributions. TG and MS designed the study. TG conducted model simulations and data analysis. RV, MC, and BA developed the GECKO-A model. YBL and PJZ conducted experimental measurements. All authors discussed the results. TG and MS wrote the manuscript with contributions from all coauthors.

Competing interests. At least one of the (co-)authors is a member of the editorial board of *Atmospheric Chemistry and Physics*. The peer-review process was guided by an independent editor, and the authors also have no other competing interests to declare.

Disclaimer. Publisher's note: Copernicus Publications remains neutral with regard to jurisdictional claims made in the text, published maps, institutional affiliations, or any other geographical representation in this paper. While Copernicus Publications makes every effort to include appropriate place names, the final responsibility lies with the authors.

Acknowledgements. This work was also funded by the U.S. Department of Energy (grant no. DE-SC0018349), the National Science Foundation (grant no. AGS-1654104), and Campus France (Make Our Planet Great Again short-stay program; grant no. mopga-short-0000000116). In addition, Paul J. Ziemann acknowledges support from the National Science Foundation (grant no. AGS-1750447).

Financial support. This research has been supported by the U.S. Department of Energy (grant no. DE-SC0018349), the National Science Foundation (grant nos. AGS-1654104 and AGS-1750447), and Campus France (grant no. mopga-short-0000000116).

Review statement. This paper was edited by Kelley Barsanti and reviewed by two anonymous referees.

References

Aimanant, S. and Ziemann, P. J.: Chemical Mechanisms of Aging of Aerosol Formed from the Reaction of n-Pentadecane with OH Radicals in the Presence of NO_x, Aerosol Sci. Technol., 47, 979–990, https://doi.org/10.1080/02786826.2013.804621, 2013a.

Aimanant, S. and Ziemann, P. J.: Development of Spectrophotometric Methods for the Analysis of Functional Groups in Oxidized Organic Aerosol, Aerosol Sci. Technol., 47, 581–591, https://doi.org/10.1080/02786826.2013.773579, 2013b.

Atkinson, R., Carter, W. P. L., Winer, A. M., and Pitts, J. N.: An Experimental Protocol for the Determination of OH Radical Rate Constants with Organics Using Methyl Nitrite Photolysis as an OH Radical Source, JAPCA J. Air Waste Ma., 31, 1090–1092, https://doi.org/10.1080/00022470.1981.10465331, 1981.

Aumont, B., Szopa, S., and Madronich, S.: Modelling the evolution of organic carbon during its gas-phase tropospheric oxidation: development of an explicit model based on a self generating approach, Atmos. Chem. Phys., 5, 2497–2517, https://doi.org/10.5194/acp-5-2497-2005, 2005.

Aumont, B., Valorso, R., Mouchel-Vallon, C., Camredon, M., Lee-Taylor, J., and Madronich, S.: Modeling SOA formation from the oxidation of intermediate volatility n-alkanes, Atmos. Chem. Phys., 12, 7577–7589, https://doi.org/10.5194/acp-12-7577-2012, 2012.

Aumont, B., Camredon, M., Mouchel-Vallon, C., La, S., Ouzebidour, F., Valorso, R., Lee-Taylor, J., and Madronich, S.: Modeling the influence of alkane molecular structure on secondary organic aerosol formation, Faraday Discuss., 165, 105–122, https://doi.org/10.1039/C3FD00029J, 2013.

Baboomian, V. J., Crescenzo, G. V., Huang, Y., Mahrt, F., Shiraiwa, M., Bertram, A. K., and Nizkorodov, S. A.: Sunlight can convert atmospheric aerosols into a glassy solid state and modify their environmental impacts, P. Natl. Acad. Sci. USA, 119, e2208121119, https://doi.org/10.1073/pnas.2208121119, 2022.

Bakker-Arkema, J. G. and Ziemann, P. J.: Minimizing Errors in Measured Yields of Particle-Phase Products Formed in Environmental Chamber Reactions: Revisiting the Yields of β-Hydroxynitrates Formed from 1-Alkene + OH/NO_x Reactions, ACS Earth and Space Chemistry, 5, 690–702, https://doi.org/10.1021/acsearthspacechem.1c00008, 2021.

Champion, W. M., Rothfuss, N. E., Petters, M. D., and Grieshop, A. P.: Volatility and Viscosity Are Correlated in Terpene Secondary Organic Aerosol Formed in a Flow Reactor, Environ. Sci. Tech. Lett., 6, 513–519, https://doi.org/10.1021/acs.estlett.9b00412, 2019.

de Gouw, J. A., Middlebrook, A. M., Warneke, C., Ahmadov, R., Atlas, E. L., Bahreini, R., Blake, D. R., Brock, C. A., Brioude, J., Fahey, D. W., Fehsenfeld, F. C., Holloway, J. S., Le Henaff, M., Lueb, R. A., McKeen, S. A., Meagher, J. F., Murphy, D. M., Paris, C., Parrish, D. D., Perring, A. E., Pollack, I. B., Ravishankara, A. R., Robinson, A. L., Ryerson, T. B., Schwarz, J. P., Spackman, J. R., Srinivasan, A., and Watts, L. A.: Organic Aerosol Formation Downwind from the Deepwater Horizon Oil Spill, Science, 331, 1295–1299, https://doi.org/10.1126/science.1200320, 2011.

DeRieux, W.-S. W., Li, Y., Lin, P., Laskin, J., Laskin, A., Bertram, A. K., Nizkorodov, S. A., and Shiraiwa, M.: Predicting the glass transition temperature and viscosity of secondary organic material using molecular composition, Atmos. Chem. Phys., 18, 6331–6351, https://doi.org/10.5194/acp-18-6331-2018, 2018.

Dette, H. P., Qi, M., Schröder, D. C., Godt, A., and Koop, T.: Glass-forming properties of 3-Methylbutane-1,2,3-tricarboxylic acid and its mixtures with water and pinonic acid, J. Phys. Chem. A, 118, 7024–7033, https://doi.org/10.1021/jp505910w, 2014.

Docherty, K. S., Wu, W., Lim, Y. B., and Ziemann, P. J.: Contributions of organic peroxides to secondary aerosol formed from reactions of monoterpenes with O_3, Environ. Sci. Technol., 39, 4049–4059, https://doi.org/10.1021/es050228s, 2005.

Evoy, E., Maclean, A. M., Rovelli, G., Li, Y., Tsimpidi, A. P., Karydis, V. A., Kamal, S., Lelieveld, J., Shiraiwa, M., Reid, J. P., and Bertram, A. K.: Predictions of diffusion rates of large organic molecules in secondary organic aerosols using the Stokes–Einstein and fractional Stokes–Einstein relations, Atmos. Chem. Phys., 19, 10073–10085, https://doi.org/10.5194/acp-19-10073-2019, 2019.

Farmer, D. K., Matsunaga, A., Docherty, K. S., Surratt, J. D., Seinfeld, J. H., Ziemann, P. J., and Jimenez, J. L.: Response of an aerosol mass spectrometer to organonitrates and organosulfates and implications for atmospheric chemistry, P. Natl. Acad. Sci. USA, 107, 6670–6675, 2010.

Galeazzo, T.: U0M0Z/tgpipe, GitHub [code], https://github.com/U0M0Z/tgpipe, last access: 6 May 2024.

Galeazzo, T. and Shiraiwa, M.: Predicting glass transition temperature and melting point of organic compounds via machine learning and molecular embeddings, Environmental Science: Atmospheres, 2, 362–374, https://doi.org/10.1039/D1EA00090J, 2022 (code available at: https://azothai.ps.uci.edu/, last access: 6 May 2024).

Galeazzo, T., Valorso, R., Li, Y., Camredon, M., Aumont, B., and Shiraiwa, M.: Estimation of secondary organic aerosol viscosity from explicit modeling of gas-phase oxidation of isoprene and α-pinene, Atmos. Chem. Phys., 21, 10199–10213, https://doi.org/10.5194/acp-21-10199-2021, 2021.

Gentner, D. R., Isaacman, G., Worton, D. R., Chan, A. W. H., Dallmann, T. R., Davis, L., Liu, S., Day, D. A., Russell, L. M., Wilson, K. R., Weber, R., Guha, A., Harley, R. A., and Goldstein, A. H.: Elucidating secondary organic aerosol from diesel and gasoline vehicles through detailed characterization of organic carbon emissions, P. Natl. Acad. Sci. USA, 109, 18318–18323, https://doi.org/10.1073/pnas.1212272109, 2012.

Grayson, J. W., Zhang, Y., Mutzel, A., Renbaum-Wolff, L., Böge, O., Kamal, S., Herrmann, H., Martin, S. T., and Bertram, A. K.: Effect of varying experimental conditions on the viscosity of α-pinene derived secondary organic material, Atmos. Chem. Phys., 16, 6027–6040, https://doi.org/10.5194/acp-16-6027-2016, 2016.

Grayson, J. W., Evoy, E., Song, M., Chu, Y., Maclean, A., Nguyen, A., Upshur, M. A., Ebrahimi, M., Chan, C. K., Geiger, F. M., Thomson, R. J., and Bertram, A. K.: The effect of hydroxyl functional groups and molar mass on the viscosity of non-crystalline organic and organic–water particles, Atmos. Chem. Phys., 17, 8509–8524, https://doi.org/10.5194/acp-17-8509-2017, 2017.

Jain, S., Fischer, B. K., and Petrucci, A. G.: The Influence of Absolute Mass Loading of Secondary Organic Aerosols on Their Phase State, Atmosphere, 9, 131, https://doi.org/10.3390/atmos9040131, 2018.

Jenkin, M. E., Valorso, R., Aumont, B., and Rickard, A. R.: Estimation of rate coefficients and branching ratios for reactions of organic peroxy radicals for use in automated mechanism construction, Atmos. Chem. Phys., 19, 7691–7717, https://doi.org/10.5194/acp-19-7691-2019, 2019.

Jenkin, M. E., Valorso, R., Aumont, B., Rickard, A. R., and Wallington, T. J.: Estimation of rate coefficients and branching ratios for gas-phase reactions of OH with aliphatic organic compounds for use in automated mechanism construction, Atmos. Chem. Phys., 18, 9297–9328, https://doi.org/10.5194/acp-18-9297-2018, 2018a.

Jenkin, M. E., Valorso, R., Aumont, B., Rickard, A. R., and Wallington, T. J.: Estimation of rate coefficients and branching ratios for gas-phase reactions of OH with aromatic organic compounds for use in automated mechanism construction, Atmos. Chem. Phys., 18, 9329–9349, https://doi.org/10.5194/acp-18-9329-2018, 2018b.

Jimenez, J. L., Canagaratna, M. R., Donahue, N. M., Prevot, A. S. H., Zhang, Q., Kroll, J. H., DeCarlo, P. F., Allan, J. D., Coe, H., Ng, N. L., Aiken, A. C., Docherty, K. S., Ulbrich, I. M., Grieshop, A. P., Robinson, A. L., Duplissy, J., Smith, J. D., Wilson, K. R., Lanz, V. A., Hueglin, C., Sun, Y. L., Tian, J., Laaksonen, A., Raatikainen, T., Rautiainen, J., Vaattovaara, P., Ehn, M., Kulmala, M., Tomlinson, J. M., Collins, D. R., Cubison, M. J., Dunlea, E. J., Huffman, J. A., Onasch, T. B., Alfarra, M. R., Williams, P. I., Bower, K., Kondo, Y., Schneider, J., Drewnick, F., Borrmann, S., Weimer, S., Demerjian, K., Salcedo, D., Cottrell, L., Griffin, R., Takami, A., Miyoshi, T., Hatakeyama, S., Shimono, A., Sun, J. Y., Zhang, Y. M., Dzepina, K., Kimmel, J. R., Sueper, D., Jayne, J. T., Herndon, S. C., Trimborn, A. M., Williams, L. R., Wood, E. C., Middlebrook, A. M., Kolb, C. E., Baltensperger, U., and Worsnop, D. R.: Evolution of organic aerosols in the atmosphere, Science, 326, 1525–1529, https://doi.org/10.1126/science.1180353, 2009.

Julin, J., Winkler, P. M., Donahue, N. M., Wagner, P. E., and Riipinen, I. A.: Near unity mass accommodation coefficient of organic molecules of varying structure, Environ. Sci. Technol., 48, 12083–12089, https://doi.org/10.1021/es501816h, 2014.

Knopf, D. A. and Alpert, P. A.: Atmospheric ice nucleation, Nat. Rev. Phys., 5, 203–217, https://doi.org/10.1038/s42254-023-00570-7, 2023.

Koop, T., Bookhold, J., Shiraiwa, M., and Pöschl, U.: Glass transition and phase state of organic compounds: dependency on molecular properties and implications for secondary organic aerosols in the atmosphere, Phys. Chem. Chem. Phys., 13, 19238–19255, 2011.

Krechmer, J. E., Pagonis, D., Ziemann, P. J., and Jimenez, J. L.: Quantification of gas-wall partitioning in Teflon environmental chambers using rapid bursts of low-volatility oxidized species generated in situ, Environ. Sci. Technol., 50, 5757–5765, 2016.

Kroll, J. H. and Seinfeld, J. H.: Chemistry of secondary organic aerosol: Formation and evolution of low-volatility organics in the atmosphere, Atmos. Environ., 42, 3593–3624, https://doi.org/10.1016/j.atmosenv.2008.01.003, 2008.

La, Y. S., Camredon, M., Ziemann, P. J., Valorso, R., Matsunaga, A., Lannuque, V., Lee-Taylor, J., Hodzic, A., Madronich, S., and Aumont, B.: Impact of chamber wall loss of gaseous organic compounds on secondary organic aerosol formation: explicit modeling of SOA formation from alkane and alkene oxidation, Atmos. Chem. Phys., 16, 1417–1431, https://doi.org/10.5194/acp-16-1417-2016, 2016.

Li, J. L., Li, K., Li, H., Wang, X. Z., Wang, W. G., Wang, K., and Ge, M. F.: Long-chain alkanes in the atmosphere: A review, J. Environ. Sci., 114, 37–52, https://doi.org/10.1016/j.jes.2021.07.021, 2022.

Li, Y., Day, D. A., Stark, H., Jimenez, J. L., and Shiraiwa, M.: Predictions of the glass transition temperature and viscosity of organic aerosols from volatility distributions, Atmos. Chem. Phys., 20, 8103–8122, https://doi.org/10.5194/acp-20-8103-2020, 2020.

Lim, Y. B. and Ziemann, P. J.: Chemistry of Secondary Organic Aerosol Formation from OH Radical-Initiated Reactions of Linear, Branched, and Cyclic Alkanes in the Presence of NO_x, Aerosol Sci. Technol., 43, 604–619, https://doi.org/10.1080/02786820902802567, 2009a.

Lim, Y. B. and Ziemann, P. J.: Effects of Molecular Structure on Aerosol Yields from OH Radical-Initiated Reactions of Linear, Branched, and Cyclic Alkanes in the Presence of NO_x, Environ. Sci. Technol., 43, 2328–2334, https://doi.org/10.1021/es803389s, 2009b.

Maclean, A. M., Smith, N. R., Li, Y., Huang, Y., Hettiyadura, A. P. S., Crescenzo, G. V., Shiraiwa, M., Laskin, A., Nizkorodov, S. A., and Bertram, A. K.: Humidity-Dependent Viscosity of Secondary Organic Aerosol from Ozonolysis of β-Caryophyllene: Measurements, Predictions, and Implications, ACS Earth and Space Chemistry, 5, 305–318, https://doi.org/10.1021/acsearthspacechem.0c00296, 2021.

Matsunaga, A. and Ziemann, P. J.: Gas-wall partitioning of organic compounds in a Teflon film chamber and potential effects on reaction product and aerosol yield measurements, Aerosol Sci. Technol., 44, 881–892, https://doi.org/10.1080/02786826.2010.501044, 2010.

McDonald, B. C., de Gouw, J. A., Gilman, J. B., Jathar, S. H., Akherati, A., Cappa, C. D., Jimenez, J. L., Lee-Taylor, J., Hayes, P. L., McKeen, S. A., Cui, Y. Y., Kim, S.-W., Gentner, D. R., Isaacman-VanWertz, G., Goldstein, A. H., Harley, R. A., Frost, G. J., Roberts, J. M., Ryerson, T. B., and Trainer, M.: Volatile chemical products emerging as largest petrochemical source of urban organic emissions, Science, 359, 760, https://doi.org/10.1126/science.aaq0524, 2018.

Mu, Q., Shiraiwa, M., Octaviani, M., Ma, N., Ding, A., Su, H., Lammel, G., Pöschl, U., and Cheng, Y.: Temperature effect on phase state and reactivity controls atmospheric multiphase chemistry and transport of PAHs, Sci. Adv., 4, eaap7314, https://doi.org/10.1126/sciadv.aap7314, 2018.

Nannoolal, Y., Rarey, J., and Ramjugernath, D.: Estimation of pure component properties – Part 3. Estimation of the vapor pressure of non-electrolyte organic compounds via group contributions and group interactions, Fluid Phase Equilibr., 269, 117–133, https://doi.org/10.1016/j.fluid.2008.04.020, 2008.

O'Brien, R. E., Li, Y., Kiland, K. J., Katz, E. F., Or, V. W., Legaard, E., Walhout, E. Q., Thrasher, C., Grassian, V. H., DeCarlo, P. F., Bertram, A. K., and Shiraiwa, M.: Emerging investigator series: chemical and physical properties of organic mixtures on indoor surfaces during HOMEChem, Environ. Sci.-Proc. Imp., 23, 559–568, https://doi.org/10.1039/D1EM00060H, 2021.

Pankow, J. F.: An absorption-model of the gas aerosol partitioning involved in the formation of secondary organic aerosol, Atmos. Environ., 28, 189–193, 1994.

Petters, S. S., Kreidenweis, S. M., Grieshop, A. P., Ziemann, P. J., and Petters, M. D.: Temperature- and Humidity-Dependent Phase States of Secondary Organic Aerosols, Geophys. Res. Lett., 46, 1005–1013, https://doi.org/10.1029/2018GL080563, 2019.

Pöschl, U. and Shiraiwa, M.: Multiphase Chemistry at the Atmosphere–Biosphere Interface Influencing Climate and Public Health in the Anthropocene, Chem. Rev., 115, 4440–4475, https://doi.org/10.1021/cr500487s, 2015.

Praske, E., Otkjær, R. V., Crounse, J. D., Hethcox, J. C., Stoltz, B. M., Kjaergaard, H. G., and Wennberg, P. O.: Atmospheric autoxidation is increasingly important in urban and suburban North America, P. Natl. Acad. Sci. USA, 115, 64–69, https://doi.org/10.1073/pnas.1715540115, 2018.

Presto, A. A., Miracolo, M. A., Donahue, N. M., and Robinson, A. L.: Secondary organic aerosol formation from high-NO_x photooxidation of low volatility precursors: n-alkanes, Environ. Sci. Technol., 44, 2029–2034, https://doi.org/10.1021/es903712r, 2010.

Pye, H. O. T., D'Ambro, E. L., Lee, B. H., Schobesberger, S., Takeuchi, M., Zhao, Y., Lopez-Hilfiker, F., Liu, J., Shilling, J. E., Xing, J., Mathur, R., Middlebrook, A. M., Liao, J., Welti, A., Graus, M., Warneke, C., de Gouw, J. A., Holloway, J. S., Ryerson, T. B., Pollack, I. B., and Thornton, J. A.: Anthropogenic enhancements to production of highly oxygenated molecules from autoxidation, P. Natl. Acad. Sci. USA, 116, 6641, https://doi.org/10.1073/pnas.1810774116, 2019.

Ranney, A. P., Longnecker, E. R., Ziola, A. C., and Ziemann, P. J.: Measured and Modeled Secondary Organic Aerosol Products and Yields from the Reaction of n-Hexadecane + OH/NO_x, ACS Earth and Space Chemistry, 7, 2298–2310, https://doi.org/10.1021/acsearthspacechem.3c00227, 2023.

Reid, J. P., Bertram, A. K., Topping, D. O., Laskin, A., Martin, S. T., Petters, M. D., Pope, F. D., and Rovelli, G.: The viscosity of atmospherically relevant organic particles, Nat. Commun., 9, 956, https://doi.org/10.1038/s41467-018-03027-z, 2018.

Renbaum-Wolff, L., Grayson, J. W., Bateman, A. P., Kuwata, K., Sellier, M., Murray, B. J., Schilling, J. E., Martin, S. T., and Bertram, A. K.: Viscosity of α-pinene secondary organic material and implications for particle growth and reactivity, P. Natl. Acad. Sci. USA, 110, 8014–8019, https://doi.org/10.1073/pnas.1219548110, 2013.

Robinson, A. L., Donahue, N. M., Shrivastava, M. K., Weitkamp, E. A., Sage, A. M., Grieshop, A. P., Lane, T. E., Pierce, J. R., and Pandis, S. N.: Rethinking organic aerosols: Semivolatile emissions and photochemical aging, Science, 315, 1259–1262, https://doi.org/10.1126/science.1133061, 2007.

Rothfuss, N. E. and Petters, M. D.: Influence of Functional Groups on the Viscosity of Organic Aerosol, Environ. Sci. Technol., 51, 271–279, https://doi.org/10.1021/acs.est.6b04478, 2017.

Saukko, E., Lambe, A. T., Massoli, P., Koop, T., Wright, J. P., Croasdale, D. R., Pedernera, D. A., Onasch, T. B., Laaksonen, A., Davidovits, P., Worsnop, D. R., and Virtanen, A.: Humidity-dependent phase state of SOA particles from biogenic and anthropogenic precursors, Atmos. Chem. Phys., 12, 7517–7529, https://doi.org/10.5194/acp-12-7517-2012, 2012.

Schervish, M. and Shiraiwa, M.: Impact of phase state and non-ideal mixing on equilibration timescales of secondary organic aerosol partitioning, Atmos. Chem. Phys., 23, 221–233, https://doi.org/10.5194/acp-23-221-2023, 2023.

Seinfeld, J. H. and Pandis, S. N.: Atmospheric chemistry and physics: from air pollution to climate change, John Wiley & Sons, ISBN 978-1-118-94740-1, 2016.

Shiraiwa, M. and Pöschl, U.: Mass accommodation and gas–particle partitioning in secondary organic aerosols: dependence on diffusivity, volatility, particle-phase reactions, and penetration depth, Atmos. Chem. Phys., 21, 1565–1580, https://doi.org/10.5194/acp-21-1565-2021, 2021.

Shiraiwa, M., Ammann, M., Koop, T., and Pöschl, U.: Gas uptake and chemical aging of semisolid organic aerosol particles, P. Natl. Acad. Sci. USA, 108, 11003–11008, https://doi.org/10.1073/pnas.1103045108, 2011.

Shiraiwa, M., Berkemeier, T., Schilling-Fahnestock, K. A., Seinfeld, J. H., and Pöschl, U.: Molecular corridors and kinetic regimes in the multiphase chemical evolution of secondary organic aerosol, Atmos. Chem. Phys., 14, 8323–8341, https://doi.org/10.5194/acp-14-8323-2014, 2014.

Shiraiwa, M., Yee, L. D., Schilling, K. A., Loza, C. L., Craven, J. S., Zuend, A., Ziemann, P. J., and Seinfeld, J. H.: Size distribution dynamics reveal particle-phase chemistry in organic aerosol formation, P. Natl. Acad. Sci. USA, 110, 11746–11750, https://doi.org/10.1073/pnas.1307501110, 2013.

Shiraiwa, M., Li, Y., Tsimpidi, A. P., Karydis, V. A., Berkemeier, T., Pandis, S. N., Lelieveld, J., Koop, T., and Pöschl, U.: Global distribution of particle phase state in atmospheric secondary organic aerosols, Nat. Commun., 8, 15002, https://doi.org/10.1038/ncomms15002, 2017.

Shrivastava, M., Lou, S., Zelenyuk, A., Easter, R. C., Corley, R. A., Thrall, B. D., Rasch, P. J., Fast, J. D., Massey Simonich, S. L., Shen, H., and Tao, S.: Global long-range transport and lung cancer risk from polycyclic aromatic hydrocarbons shielded by coatings of organic aerosol, P. Natl. Acad. Sci. USA, 114, 1246–1251, 2017.

Smith, N. R., Crescenzo, G. V., Huang, Y., Hettiyadura, A. P. S., Siemens, K., Li, Y., Faiola, C. L., Laskin, A., Shiraiwa, M., Bertram, A. K., and Nizkorodov, S. A.: Viscosity and liquid–liquid phase separation in healthy and stressed plant SOA, Environmental Science: Atmospheres, 1, 140–153, https://doi.org/10.1039/D0EA00020E, 2021.

Song, M., Maclean, A. M., Huang, Y., Smith, N. R., Blair, S. L., Laskin, J., Laskin, A., DeRieux, W.-S. W., Li, Y., Shiraiwa, M., Nizkorodov, S. A., and Bertram, A. K.: Liquid–liquid phase separation and viscosity within secondary organic aerosol generated from diesel fuel vapors, Atmos. Chem. Phys., 19, 12515–12529, https://doi.org/10.5194/acp-19-12515-2019, 2019.

Srivastava, D., Vu, T. V., Tong, S., Shi, Z., and Harrison, R. M.: Formation of secondary organic aerosols from anthropogenic precursors in laboratory studies, npj Climate and Atmospheric Science, 5, 22, https://doi.org/10.1038/s41612-022-00238-6, 2022.

Tobias, H. J., Kooiman, P. M., Docherty, K. S., and Ziemann, P. J.: Real-Time Chemical Analysis of Organic Aerosols Using a Thermal Desorption Particle Beam Mass Spectrometer, Aerosol Sci. Technol., 33, 170–190, https://doi.org/10.1080/027868200410912, 2000.

Valorso, R., Aumont, B., Camredon, M., Raventos-Duran, T., Mouchel-Vallon, C., Ng, N. L., Seinfeld, J. H., Lee-Taylor, J., and Madronich, S.: Explicit modelling of SOA formation from α-pinene photooxidation: sensitivity to vapour pressure estimation, Atmos. Chem. Phys., 11, 6895–6910, https://doi.org/10.5194/acp-11-6895-2011, 2011.

Vereecken, L. and Peeters, J.: Decomposition of substituted alkoxy radicals–part I: a generalized structure–activity relationship for reaction barrier heights, Phys. Chem. Chem. Phys., 11, 9062–9074, 2009.

Verwer, J. G.: Gauss–Seidel iteration for stiff ODEs from chemical kinetics, SIAM J. Sci. Comput., 15, 1243–1250, 1994.

Verwer, J. G., Blom, J. G., and Hundsdorfer, W.: An implicit-explicit approach for atmospheric transport-chemistry problems, Appl. Numer. Math., 20, 191–209, 1996.

Virtanen, A., Joutsensaari, J., Koop, T., Kannosto, J., YliPirilä, P., Leskinen, J., Mäkelä, J. M., Holopainen, J. K., Pöschl, U., Kulmala, M., Worsnop, D. R., and Laaksonen, A.: An amorphous solid state of biogenic secondary organic aerosol particles, Nature, 467, 824–827, https://doi.org/10.1038/nature09455, 2010.

Ye, Q., Robinson, E. S., Ding, X., Ye, P., Sullivan, R. C., and Donahue, N. M.: Mixing of secondary organic aerosols versus relative humidity, P. Natl. Acad. Sci. USA, 113, 12649–12654, 2016.

Zaveri, R. A., Wang, J., Fan, J., Zhang, Y., Shilling John, E., Zelenyuk, A., Mei, F., Newsom, R., Pekour, M., Tomlinson, J., Comstock Jennifer, M., Shrivastava, M., Fortner, E., Machado Luiz, A. T., Artaxo, P., and Martin Scot, T.: Rapid growth of anthropogenic organic nanoparticles greatly alters cloud life cycle in the Amazon rainforest, Sci. Adv., 8, eabj0329, https://doi.org/10.1126/sciadv.abj0329, 2022.

Zhang, X., Cappa, C. D., Jathar, S. H., McVay, R. C., Ensberg, J. J., Kleeman, M. J., and Seinfeld, J. H.: Influence of vapor wall loss in laboratory chambers on yields of secondary organic aerosol, P. Natl. Acad. Sci. USA, 111, 5802–5807, 2014.

Zhang, Y., Chen, Y., Lambe, A. T., Olson, N. E., Lei, Z., Craig, R. L., Zhang, Z., Gold, A., Onasch, T. B., Jayne, J. T., Worsnop, D. R., Gaston, C. J., Thornton, J. A., Vizuete, W., Ault, A. P., and Surratt, J. D.: Effect of the Aerosol-Phase State on Secondary Organic Aerosol Formation from the Reactive Uptake of Isoprene-Derived Epoxydiols (IEPOX), Environ. Sci. Tech. Lett., 5, 167–174, https://doi.org/10.1021/acs.estlett.8b00044, 2018.

Zhang, Y., Nichman, L., Spencer, P., Jung, J. I., Lee, A., Heffernan, B. K., Gold, A., Zhang, Z., Chen, Y., Canagaratna, M. R., Jayne, J. T., Worsnop, D. R., Onasch, T. B., Surratt, J. D., Chandler, D., Davidovits, P., and Kolb, C. E.: The Cooling Rate- and Volatility-Dependent Glass-Forming Properties of Organic Aerosols Measured by Broadband Dielectric Spectroscopy, Environ. Sci. Technol., 53, 12366–12378, https://doi.org/10.1021/acs.est.9b03317, 2019.

Zhao, B., Wang, S., Donahue, N. M., Jathar, S. H., Huang, X., Wu, W., Hao, J., and Robinson, A. L.: Quantifying the effect of organic aerosol aging and intermediate-volatility emissions on regional-scale aerosol pollution in China, Sci. Rep., 6, 28815, https://doi.org/10.1038/srep28815, 2016.

Zhou, S., Hwang, B. C. H., Lakey, P. S. J., Zuend, A., Abbatt, J. P. D., and Shiraiwa, M.: Multiphase reactivity of polycyclic aromatic hydrocarbons is driven by phase separation and diffusion limitations, P. Natl. Acad. Sci. USA, 116, 11658–11663, https://doi.org/10.1073/pnas.1902517116, 2019.

Ziemann, P. J. and Atkinson, R.: Kinetics, products, and mechanisms of secondary organic aerosol formation, Chem. Soc. Rev., 41, 6582–6605, 2012.

Zobrist, B., Marcolli, C., Pedernera, D. A., and Koop, T.: Do atmospheric aerosols form glasses?, Atmos. Chem. Phys., 8, 5221–5244, https://doi.org/10.5194/acp-8-5221-2008, 2008.